Int. J. Electron. Commun. (AEÜ) 138 (2021) 153875

Contents lists available at ScienceDirect

International Journal of Electronics and Communications

journal homepage: www.elsevier.com/locate/aeue

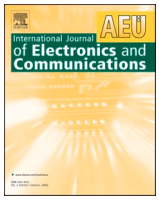

Regular paper

Extreme learning machine detector for millimeter-wave massive MIMO systems

Diego Fernando Carrera [a,*], Cesar Vargas-Rosales [b], Cesar A. Azurdia-Meza [c], Marco Morocho-Yaguana [d]

[a] Research Department, Universidad Tecnológica Empresarial de Guayaquil, Guayaquil 090511, Ecuador
[b] School of Engineering and Sciences, Tecnológico de Monterrey, Monterrey 64849, Mexico
[c] Department of Electrical Engineering, Universidad de Chile, Santiago 8370451, Chile
[d] Department of Computer Science and Electronics, Universidad Tecnica Particular de Loja, Loja 110107, Ecuador

ARTICLE INFO

Keywords:
5G and beyond
ELM
Massive MIMO
mm-wave

ABSTRACT

In this paper, we present an extreme learning machine (ELM) neural network designed to perform multiple-input multiple-output (MIMO) detection for millimeter-wave (mm-wave) communications operating in the 28 GHz frequency band. The ELM strategy can perform online MIMO combining processing. This method does not require offline training like with deep neural networks. The proposed technique was compared in terms of the achievable bit error rate (BER) and spectral efficiency (SE) to the maximum ratio (MR) and minimum mean squared error (MMSE) MIMO detectors, considering an orthogonal frequency-division multiplexing (OFDM) uplink scheme based on the fifth generation (5G) New Radio standard. Numerical results show that the ELM strategy outperforms the MR and MMSE detectors since this method reduces the inter-user interference effects, specifically for low equivalent isotropic radiated power at the receiver during the uplink communication. Furthermore, the ELM method requires only 16 % of the floating-point operations required by the MMSE detector.

1. Introduction

Millimeter wave (mm-wave) communications could take two to five years to become a mainstream technology used by end users [1]. This is due to the limited range of coverage, which requires a dense deployment of radio equipment, resulting in a high investment for mobile service providers. However, the fifth generation (5G) ultra-wideband (UWB) standard, which defines the mm-wave frequency band for mobile communications, has impressed with the data transfer speeds that can be achieved.

From the operator's point of view, what is desired is greater coverage of the base station (BS) to increase the intercell site distance (ISD), since the greater the distance between cells, fewer BSs are required, therefore, the capital expenditure (CAPEX) and the operational expenditure (OPEX) can be reduced. The author in [2] has determined that a mm-wave BS can cover an ISD of 1000 meters, although this is only true for the downlink (DL) communication, meaning that this distance is possible when the BS transmits towards the users, not when the users transmit to the BS. However, in the uplink (UL) communication, the ISD distance is reduced to only 250 meters. This phenomenon manifests because, in the DL, the BS can transmit the mm-wave signal with a higher power in comparison to the one used by the users when transmitting towards the BS. This is because the users use mobile devices that are limited in power. Since mm-wave communications occur in both the UL and the DL, an ISD of 1000 meters cannot be covered since the UL restricts this distance to a quarter of the coverage range of the DL.

Another challenge during the UL communications with mm-wave systems is the inter-user interference, which can reduce the spectral efficiency (SE) of the wireless link. This phenomenon is hard to resolve with linear multiple-input multiple-output (MIMO) detectors such as the maximum ratio (MR) and minimum mean squared error (MMSE) techniques. Therefore, optimized signal processing schemes are required to reduce the latency and establish a reliable communication link even for systems with low power signals. However, complex techniques suppose higher computational complexity. This is where artificial intelligence methods become handy since many applications designed with neural networks have been successful in optimizing the 5G network [3].

On the other hand, in recent years, we have seen great advances in

* Corresponding author.
E-mail address: dfcarrera@ieee.org (D.F. Carrera).

https://doi.org/10.1016/j.aeue.2021.153875
Received 2 April 2021; Accepted 18 June 2021
Available online 24 June 2021

artificial intelligence algorithms like deep neural networks (DNNs) in many areas that involve mobile communications. However, the biggest obstacle for mm-wave communications is at the network edge, where optimized signal processing is required to reduce the latency and establish a communication link even at low signal power.

The work in [4] considers two artificial neural networks (ANNs) strategies, namely, the extreme learning machine (ELM) and a multilayer perceptron (MLP). Both techniques were used to perform channel equalization for mm-wave signals. Although the study is limited to single-input single-output (SISO) systems. The ELM strategy can perform channel equalization online, whereas the MLP method requires offline training and the performance is limited to the algorithm used to train the MLP network.

The work in [5] presents an ELM neural network for orthogonal frequency division multiplexing (OFDM) links that do not use MIMO technology. On the other hand, the ELM method has been reported to be successful on massive MIMO systems, which are fundamental for mm-wave communication systems [6]. However, these studies do not consider the use of mm-waves in the communication link, where hybrid arrays of antennas are the rule, such as partially and fully connected arrays, to establish a beamforming link [7].

The work in [8] presents the foundation for and ELM design applied to massive MIMO systems, which are the base technology for beamforming mm-wave systems. However, this work is limited to sub-6 GHz bands, where the hybrid beamforming processing is not considered. The study in [8] can be also related to the work in [9], where an adaptive ELM receiver is designed to handle both the LED nonlinearity and cross-LED interference in MIMO LED communications. Here the activation function is the sigmoid function and the design was defined in the real domain. Both works are limited to the symbol error rate analysis.

Hybrid beamforming allows the steering of narrow signal beams towards users with reduced complexity thanks to the separation of the analog and digital domains. This architecture requires the establishment of a beamforming link between the BS and multiple users in the network. However, beam selection is a time-consuming process [10]. Due to the digital processing part of hybrid beamforming, ANNs have the potential to adapt to many hybrid array structures and reduce the complexity of the signal processing task [11,12].

In this study, we propose the use of ELM neural networks to tackle the problem of mm-wave links with high path loss, considering a partially connected hybrid array of antennas at the BS since this array structure is less expensive than a fully connected one and requires significantly less power, so is widely used in commercial mm-wave radios [7,13]. Specifically, we study the problem of detecting massive MIMO signals in high path loss scenarios during UL communication. For this, we adjusted the equivalent isotropic radiated power (EIRP) between the BS and the users in the cell. We compared the proposed ELM scheme in terms of achievable SE, bit error rate (BER), and number floating-point operations to the performance of the MR and MMSE detectors, two common MIMO combining techniques found in the literature [14]. Numerical results show the ELM design can achieve higher SE and lower BER even with a low EIRP link. With this, there is the potential to increase the coverage of UL mm-wave communications and increase the ISD between BSs. The contributions of this work are summarized as follows:

- We use a fully complex ELM-based detector for mmWave communications, where the ELM training is performed by learning the optimal combiner process as is introduced in 2.1.
- We test the performance of the proposed ELM detector by changing the EIRP of the UL mmWave link. This way, we analyzed the performance for mmWave links with low signal power (EIRP $= 10$ dB) and high signal power (EIRP $= 20$ dB).
- We proved that the proposed ELM detector automatically adapts to the hybrid beamforming of the mmWave system without requiring extra configurations.

The remainder of this work is organized as follows. Section 2 presents the mm-wave system and channel model. The proposed ELM neural network is outlined in Section 3. In Section 4, the numerical results of the proposed solution are presented, whereas the results are discussed in Section 5. Finally, concluding remarks are given in Section 6.

2. System Model

In this section, we present the mm-wave system and channel model considered in this study.

2.1. Mm-wave system model

We consider a partially connected hybrid massive MIMO BS which communicates with K users based on cyclic prefix (CP) OFDM communication links, as shown in Fig. 1.

The left-hand side of Fig. 1 shows a partially connected hybrid array mm-wave BS composed of R transceivers (RF chains) and $M = RN_{\mathrm{r}}$ antennas. Each RF chain is connected to a subarray of N_{r} antennas trough analog RF precoders (phase shifters), this way, $K \leqslant R$ users can be simultaneously multiplexed with this hybrid structure. The right-hand side of Fig. 1 shows the K users, where analog precoding is performed over N_{t} RF paths. At the transmitter (the k^{th} user), a digital baseband beamformer (precoder) $\mathbf{f}_{\mathrm{BB}_k} \in \mathbb{C}^{N_{\mathrm{t}} \times 1}$ is used to precode N_{s} data symbols followed by an analog precoder $\mathbf{F}_{\mathrm{RF}_k} = \mathrm{diag}\left(f_{k1}^{\mathrm{par}}, f_{k2}^{\mathrm{par}}, \ldots, f_{kN_{\mathrm{t}}}^{\mathrm{par}}\right)$, where $f_{kN_{\mathrm{t}}}^{\mathrm{par}}$ is the RF precoder matrix element for the partially connected hybrid array [13,15,7]. We assumed that a beam steering RF codebook is used by the BS to select the k^{th} RF combiner, $\mathbf{W}_{rf_k}^{*}$, during the beam-sweeping process, which is required to establish the links between the K multiplexed users and the mm-wave BS [16,17].

In practical mm-wave systems, the channel state information (CSI) is estimated via UL training with pilots transmitted from multiple users [18,14]. The combining vector can be found with the estimated CSI, so the MIMO detection process can be performed on the received signals in the digital domain [19,20]. In this study, we considered the least square (LS) channel estimator, a simple and fast way to estimate the CSI [21,20].

The mm-wave MIMO OFDM system employs $n = 1, \ldots, N_{\mathrm{s}}$ subcarriers to transmit the data symbols, where N_{s} is the number of subcarriers. In the UL, the n^{th} subcarrier reference signal $\mathbf{y}_k^x[n] \in \mathbb{C}^{N_{\mathrm{r}}}$ received at the r^{th} RF chain of the BS and transmitted by the k^{th} user is given by

$$\mathbf{y}_k^x[n] = \sqrt{\rho_k}\mathbf{W}_{rf_k}^{*}\mathbf{H}_k[n]\mathbf{F}_{\mathrm{RF}_k}\mathbf{f}_{\mathrm{BB}_k}[n]x_k[n] + \sum_{\substack{j=1 \\ j \neq k}}^{K} \sqrt{\rho_j}\mathbf{W}_{rf_k}^{*}\mathbf{H}_j[n]\mathbf{F}_{\mathrm{RF}_j}\mathbf{f}_{\mathrm{BB}_j}[n]x_j[n] + \mathbf{W}_{rf_k}^{*}\mathbf{v}_k[n], \quad (1)$$

where $\mathbf{H}_k[n], \mathbf{H}_j[n] \in \mathbb{C}^{N_{\mathrm{r}} \times N_{\mathrm{t}}}$ are the n^{th} subcarrier massive MIMO channel coefficients established between the k^{th} and j^{th} users and the BS, respectively. $\mathbf{F}_{\mathrm{RF}_k}\mathbf{f}_{\mathrm{BB}_k}[n]$ denotes the n^{th} subcarrier precoder for the k^{th} user, whereas $\mathbf{F}_{\mathrm{RF}_j}\mathbf{f}_{\mathrm{BB}_j}[n]$ denotes the n^{th} subcarrier precoder for the j^{th} interfering user. $x_k[n]$ is n^{th} subcarrier transmitted pilot from the k^{th} user, whereas $x_j[n]$ denotes the n^{th} subcarrier transmitted pilot from the j^{th} user. Since all pilots are independent, $\mathbb{E}\left[\left|\mathbf{x}_k\right|^2\right] = \rho_k$ for $k = 1, 2, \ldots, K$, and $\mathbb{E}\left[\left|\mathbf{x}_j\right|^2\right] = \rho_j$ for $j = 1, 2, \ldots, K. j \neq k$, where ρ_k and ρ_j represent the transmission power of the k^{th} and j^{th} users, respectively. Lastly, $\mathbf{v}_k[n] \in \mathbb{C}^{N_{\mathrm{r}}}$ represents the i.i.d $\mathscr{CN}\left(0, \sigma_{\mathbf{v}_k}^2\right)$ additive noise vector [15,18].

By defining the k^{th} effective channel of the desired user as $\mathbf{h}_{\mathrm{eff}_k}[n] = \mathbf{W}_{rf_k}^{*}\mathbf{H}_k[n]\mathbf{F}_{\mathrm{RF}_k}\mathbf{f}_{\mathrm{BB}_k}[n]$, and the j^{th} effective interfering channel as $\mathbf{h}_{\mathrm{eff}_j}[n] = \mathbf{W}_{rf_k}^{*}\mathbf{H}_j[n]\mathbf{F}_{\mathrm{RF}_j}\mathbf{f}_{\mathrm{BB}_j}[n]$, the received data signal is given by

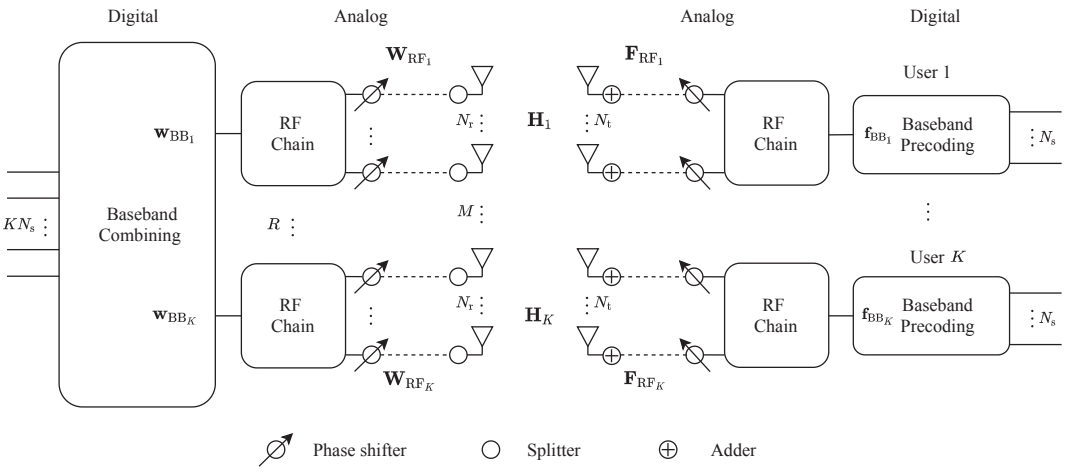

Fig. 1. Simplified system blocks of an UL multiuser mm-wave system with a partially connected hybrid array of antennas. On the left-hand side is represented the mm-wave BS and on the right-hand side are represented K multi-antenna users.

$$\mathbf{y}_k^s[n] = \mathbf{h}_{\mathrm{eff}_k}[n]s_k[n] + \sum_{\substack{j=1 \\ j\neq k}}^{K} \mathbf{h}_{\mathrm{eff}_j}[n]s_j[n] + \mathbf{W}_{rf_k}^{*}\mathbf{v}_k[n], \tag{2}$$

where $s_k[n]$ denotes the data symbol transmitted from the desired k^{th} user, whereas $s_j[n]$ represents the data symbols from the j^{th} interfering user.

Therefore, the MIMO detection problem reduces to finding a combining vector that recovers the transmitted data symbols as follows

$$\widehat{s}_k[n] = \mathbf{w}_{bb_k}^{*}[n]\mathbf{h}_{\mathrm{eff}_k}[n]s_k[n] + \sum_{\substack{j=1 \\ j\neq k}}^{K} \sqrt{\mathbf{w}}_{\mathbf{bb_k}}^{*}[\mathbf{n}]\mathbf{h}_{\mathrm{eff_j}}[\mathbf{n}]\mathbf{s_j}[n] + \mathbf{w}_{bb_k}^{*}[n]\mathbf{W}_{rf_k}^{*}\mathbf{v}_k[n], \tag{3}$$

where $\mathbf{w}_{bb_k}^{*}[n]$ is the k^{th} baseband (BB) combiner that maximizes the data symbol power, forcing to zero the interfering, additive noise, and nonlinear distortion signals. This problem is hard to resolve with linear MIMO detectors like MR and MMSE. The MR detector maximizes the desired signal power, but it does not filter inter-user interference or nonlinear distortions. On the other hand, the MMSE detector can partially reduce the interference effects, performing better than the MR method [22]. Although a complete attenuation of the inter-user interference and nonlinear distortion effects is desired, which can only be achieved with the optimal combiner $\mathbf{w}_{\mathrm{opt}_k}[n] \in \mathbb{C}^{N_r\times 1}$, which is given by [18]

$$\begin{aligned} \mathbf{w}_{\mathrm{opt}_k}[n] &= \operatorname{argmin} \mathbb{E}\left[\left\| s_k[n] - \mathbf{w}_{\mathrm{opt}_k}^{*}\mathbf{y}_k^s[n]\right\|^2\right], \\ &\text{s.t. } \mathbf{w}_{\mathrm{opt}_k}^{*}[n]\mathbf{h}_{\mathrm{eff}_i}[n] = \begin{cases} c1, i = k \\ 0, i \neq k. \end{cases} \end{aligned} \tag{4}$$

The optimal combining process in (4) allows to maximize the k^{th} signal power, the signal from the desired user, while filtering the interfering signals and noise. Linear MIMO combiners, like MR or MMSE, are processed with the estimated CSI of k^{th} user. However, the information of the interfering sources is not available, so the detection is not optimal. Thus, new strategies like ANNs have the potential to perform the MIMO detection task by learning the optimal combiner process.

2.2. Channel model

For simplicity, we avoid the use of subscripts defined for the channel matrices $\mathbf{H}_k[n]$, and $\mathbf{H}_j[n]$. Therefore, in this subsection, we describe a general mm-Wave MIMO channel. Using the clustered channel model described in [18,23], the delay tap d^{th} of discrete-time $N_r \times N_t$ channel matrix $\mathbf{H}_d$ for $d = 1, \ldots, N_c$ is written as

$$\mathbf{H}_d = \sqrt{\frac{N_r N_t}{N_{cl} N_{ray}}} \sum_{\eta=1}^{N_{cl}} \sum_{\iota=1}^{N_{ray}} g_{\eta\iota}\mathbf{a}_r\left(\theta_{\eta\iota}^r, \phi_{\eta\iota}^r\right)\mathbf{a}_t^h\left(\theta_{\eta\iota}^t, \phi_{\eta\iota}^t\right), \tag{5}$$

where $g_{\eta\iota}$ is the complex small-scale fading gain of the ι^{th} ray in the η^{th} scattering cluster, characterized as i.i.d. $\mathscr{CN}(0, \sigma_\eta^2)$, and σ_η^2 denotes the average power of the η^{th} cluster. N_{cl} is the number of scattering clusters, whereas N_{ray} is the number of rays (subpaths). The vectors $\mathbf{a}_r\left(\theta_{\eta\iota}^r, \phi_{\eta\iota}^r\right)$ and $\mathbf{a}_t^h\left(\theta_{\eta\iota}^t, \phi_{\eta\iota}^t\right)$ denote the array response functions, for the receive and transmit antenna arrays, with respect to the angles of arrival $\phi_{\eta\iota}^r\left(\theta_{\eta\iota}^r\right)$ and departure $\phi_{\eta\iota}^t\left(\theta_{\eta\iota}^t\right)$, respectively. Finally, as in [21], the frequency channel response at the subcarrier n, in terms of N_c delay taps in the discrete-time domain is given by

$$\mathbf{H}[n] = \sum_{d=1}^{N_c} \mathbf{H}_d e^{-j\frac{2\pi n}{N_s}d}. \tag{6}$$

3. ELM neural network

With the proposed ELM strategy, the objective is to detect the MIMO signal as well as the optimal combiner in (4). To do so, the ELM can be applied in the complex domain taking as input the received pilot signal vector $\mathbf{Y}_k^x = \left\{\mathbf{y}_k^x[1], \ldots, \mathbf{y}_k^x[N_s]\right\}^t$ and as output the pilot vector $\mathbf{x}_k = \left\{x_k[1], \ldots, x_k[N_s]\right\}^t$, a priori known at the BS, as is illustrated in Fig. 2. This way, only the desired signal is maximized while the interference signals are attenuated.

For the case of hybrid beamforming, channel estimation, and therefore MIMO combining must be performed on the digital baseband received signal $\mathbf{y}_{bb_k}^x[s]$. Thus, the RF combining matrix must be filtered out from $\mathbf{y}_k^x[n]$, to do so, the operation is given by

$$\mathbf{y}_{bb_k}^x[n] = \left[\mathbf{W}_{rf_k}\mathbf{W}_{rf_k}^{*}\right]^{-1}\mathbf{W}_{rf_k}\mathbf{y}_k^x[n]. \tag{7}$$

But, channel estimation is a process that is required by linear MIMO detectors, namely, MR and MMSE. However, the ELM neural network does not require to perform channel estimation, although this method requires to adapt to different beamforming designs, namely, fully connected, partially connected, subconnected, among other hybrid structure designs, even dynamic hybrid beamforming [24]. In other words,

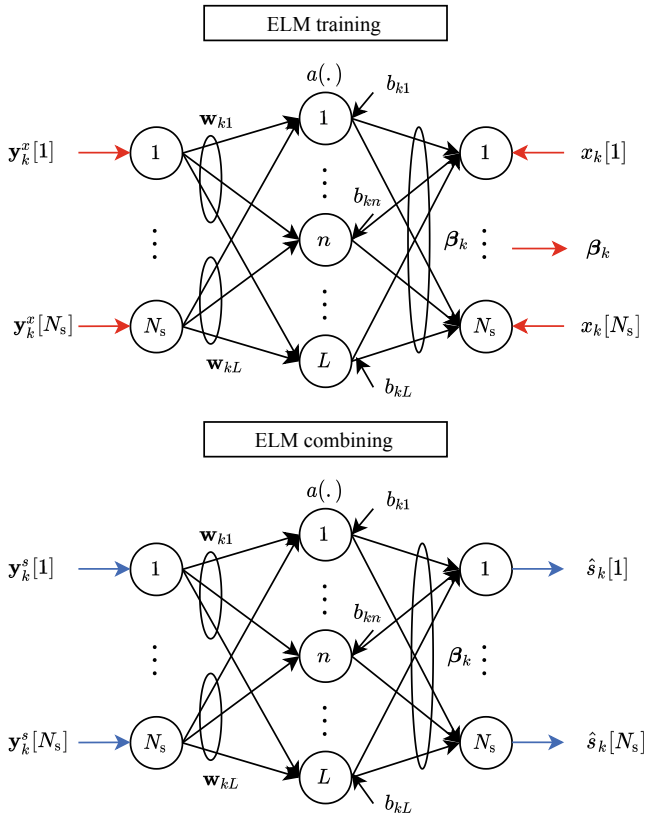

Fig. 2. Structure of the ELM detector. The received pilot signal matrix $\mathbf{Y}_r^x$ and the pilot symbols $\mathbf{x}_k$ are used for online training of the ELM neural network in order to find the output weight vector $\boldsymbol{\beta}_k$, and then the received data symbols $\mathbf{Y}_r^s$ can be directly combined.

there is no need to filter out the RF combining matrix to train the proposed ELM method.

The advantage of the ELM neural network is that it can perform MIMO detection online. Namely, it is not required to train the ELM network offline like with traditional DNN strategies [5,6]. DNN algorithms take batches of training data to train a model, the neural network then predicts the test sample using the found relationship. This process takes considerable computational processing and cannot be performed online. Whereas online learning takes an initial guess model and then picks up one by one observation from the training data and recalibrates the weights of each input parameter. This process allows the algorithm to dynamically adapt to new patterns in the data, like different hybrid beamforming designs. In this case, the ELM method dynamically adapts to the changes in the mmWave channel fast and with low computational complexity [25].

The k^{th} ELM detector, which consist of L hidden nodes, between the input and the output layers is given by $\mathbf{x}_k = \mathbf{O}_{x,k}\boldsymbol{\beta}_k$, where $\boldsymbol{\beta}_k \in \mathbb{C}^L$ is the output weight vector, and $\mathbf{O}_{x,k} \in \mathbb{C}^{N_s \times L}$ represents the hidden layer output matrix when the pilot signal matrix $\mathbf{Y}_k^x$ is used at the input of the ELM neural network. $\mathbf{O}_{x,k}$ is given by

$$\mathbf{O}_{x,k} = \begin{bmatrix} a(\mathbf{w}_{k1}^t \mathbf{y}_k^x[1] + b_{k1}) & \cdots & a(\mathbf{w}_{kL}^t \mathbf{y}_k^x[1] + b_{kL}) \\ \vdots & \ddots & \vdots \\ a(\mathbf{w}_{k1}^t \mathbf{y}_k^x[N_s] + b_{k1}) & \cdots & a(\mathbf{w}_{kL}^t \mathbf{y}_k^x[N_s] + b_{kL}) \end{bmatrix}, \tag{8}$$

where $a(\cdot)$ is the activation function of the hidden layer. k^{th} input weights $\mathbf{w}_{kn} = [w_{kn1}, \ldots, w_{knN_r}]^t \in \mathbb{C}^{N_r}$ and biases b_{kn} of the n^{th} hidden node, for $n = 1, \ldots, L$, are randomly initialized and fixed without tuning for the ELM training step. Specifically, when $N_s > L$, the output weight vector is written as

$$\boldsymbol{\beta}_k = \left(\mathbf{O}_{x,k}^h \mathbf{O}_{x,k}\right)^{-1} \mathbf{O}_{x,k}^h \mathbf{x}_k. \tag{9}$$

After the ELM detector is trained, we can use the data signal $\mathbf{Y}_k^s = \{\mathbf{y}_k^s[1], \ldots, \mathbf{y}_k^s[N_s]\}^t$ at the input of the neural network as is illustrated in Fig. 2 [8]. Therefore, a new data output weight vector $\mathbf{O}_{s,k} \in \mathbb{C}^{N_s \times L}$ is processed as

$$\mathbf{O}_{s,k} = \begin{bmatrix} a(\mathbf{w}_{k1}^t \mathbf{y}_k^s[1] + b_{k1}) & \cdots & a(\mathbf{w}_{kL}^t \mathbf{y}_k^s[1] + b_{kL}) \\ \vdots & \ddots & \vdots \\ a(\mathbf{w}_{k1}^t \mathbf{y}_k^s[N_s] + b_{k1}) & \cdots & a(\mathbf{w}_{kL}^t \mathbf{y}_k^s[N_s] + b_{kL}) \end{bmatrix}. \tag{10}$$

Finally, the last step is to perform MIMO combining with the trained ELM output weight vector as follows

$$\widehat{\mathbf{s}}_k = \mathbf{O}_{s,k}\boldsymbol{\beta}_k, \tag{11}$$

where $\widehat{\mathbf{s}}_k = \{\widehat{s}_k[1], \ldots, \widehat{s}_k[N_s]\}^t$ denotes the detected data symbols at the output layer of the ELM network [6,26]. It is worth nothing that $\mathbf{w}_{kn}$ and b_{kn} in (8) are fixed after the ELM training and reused in (10).

4. Simulation results

We first define the radio link parameters used in our simulations for mm-wave communications with a partially connected hybrid array of antennas for the 28 GHz frequency band, based on the 3GPP Release 15 standard, as summarized in Table 1 [17]. The channel between the K user and the BS was simulated with the quasi-deterministic radio channel generator (QuaDRiGa) [27], using the mmMAGIC Non-Line-of-Sight (NLoS) [28], a cluster channel model developed exclusively for mmWave scenarios, as is described in Section 2.2.

We ran a multiuser mm-wave communication following the 5G NR Type I pilot mapping structure, where one OFDM symbol is used for pilot mapping, as is illustrated in Fig. 3.

The pilot structure shown in Fig. 3 allows the multiplexing of up to four users. However, up to 12 users can be multiplexed with a different pilot mapping structure, and 5G NR defines that pilots are mapped to quadrature phase-shift keying (QPSK) modulation.

For the ELM detector, the pilots must follow the same modulation

Table 1
Simulation parameters.

Parameter	Value
BS height	10 m
BS position	0, 0 (x,y coordinates in [m])
Users height	1.5 m for each user
Users position	random to the east-side of the BS
Channel model	mmMagic NLoS
User device antenna array configuration	dual-antenna devices
Cell radius	125 m
Carrier frequency	28 GHz
Carrier type	CP-OFDM (120 kHz of subcarrier spacing)
Carrier bandwidth	100 MHz
NR data slot	12 subcarriers per PRB, 14 OFDM symbols per slot/ subframe, 66 PRBs
Occupied subcarriers	792 subcarriers per OFDM symbol
Channel estimation	MMSE
MIMO processing	MR, MMSE and ELM
Maximum path loss	125.5 dB
Fully-connected BS antenna properties	
Number of antenna panels	1
Number of antenna elements per panel	16 × 16 array with dual polarization (256T256R per polarization, $M = 512$)
Element separation distance	0.5λ
Number of RF chains/ beams	8
Peak beam gain (dBi)	27

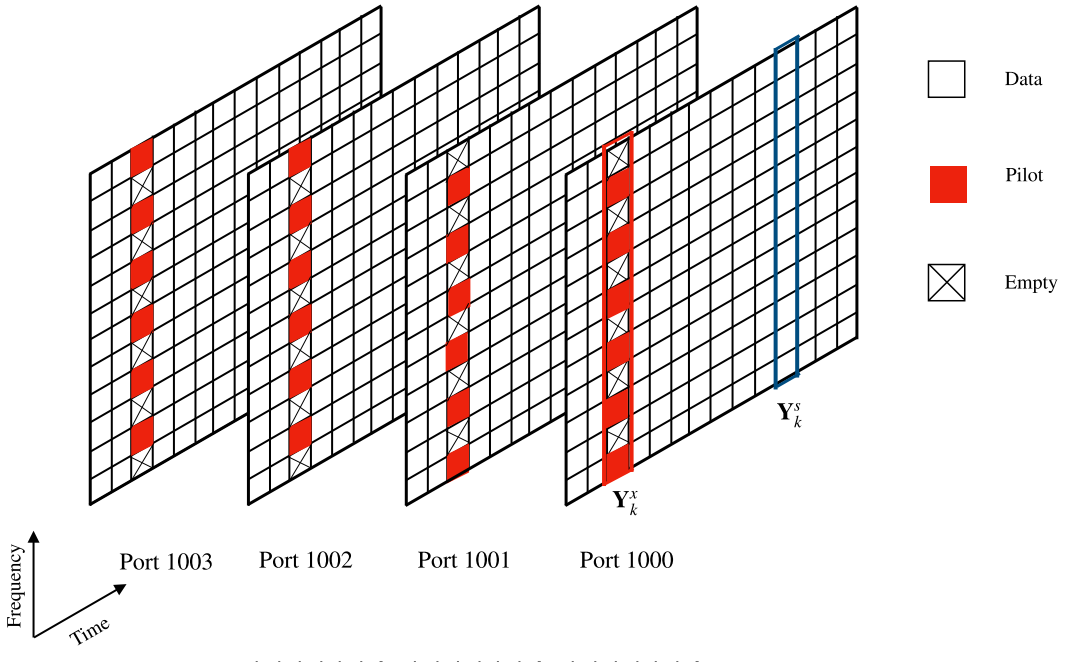

Fig. 3. 5G NR Type I multiuser pilot mapping. Four users are assigned an antenna port from 1000 to 1003.

scheme as the data symbols to achieve the maximum wireless performance [5,6]. Therefore, in this work, we chose the quadrature phase shift keying (QPSK), 16-quadrature amplitude modulation (16-QAM), and 64-QAM as the modulation schemes with a channel coding based on the low-density parity check (LDPC) scheme with a target code rate of 449/1024, 616/1024 and 764/1024, respectively [17]. Results are different for every modulation scheme; however, 64-QAM is more sensitive to high path loss, like the one present in mm-wave scenarios since this modulation requires high SNR values to obtain low BER [6].

We set the ELM neural network with a *tanh* activation function, and the weights and biases were arbitrarily generated following a uniform distribution in the interval [-1,1], which consists of the activation function region of convergence, widely utilized in ANNs [6,5]. We also set the number of hidden neurons equal to the number of antennas of the partially connected panel array at the BS as $L = N_{\mathrm{r}}$ [6]. With these parameters, we performed the simulations based on the radio links between the BS and the users with two fixed EIRPs on the transmitter side. The EIRP value is given by [2]

$$\mathrm{EIRP} = P_{\mathrm{sensitivity}} + \mathrm{SNR} - G_a + PL, \tag{12}$$

where $P_{\mathrm{sensitivity}}$ denotes the receiver sensitivity, which is equivalent to -99.2 dBm for mmWave communications. G_a is the receiver antenna gain and is given by the peak beam gain, which is 24 dBi, whereas PL denotes the path loss generated with the mmMagic channel model of the QuaDRiGa simulator [29,27]. For the UL communication, the maximum EIRP is 20 dBm for a 100 MHz channel link [2].

Figs. 4–6 show the average SE and BER results for a fixed EIRP of 10 dBm with the QPSK, 16QAM, and 64-QAM modulation schemes, respectively.

Figs. 4–6 show that the ELM detector outperforms the MR and MMSE techniques since the achievable BER is significantly smaller for the former. Although, the SE results for the QPSK modulation are smaller for the ELM detector. The results also show that the ELM method can reliably detect the MIMO signal with smaller BER even for a low EIPR of 10 dBm.

Figs. 7–9 show the average SE and BER results for a fixed EIRP of 20

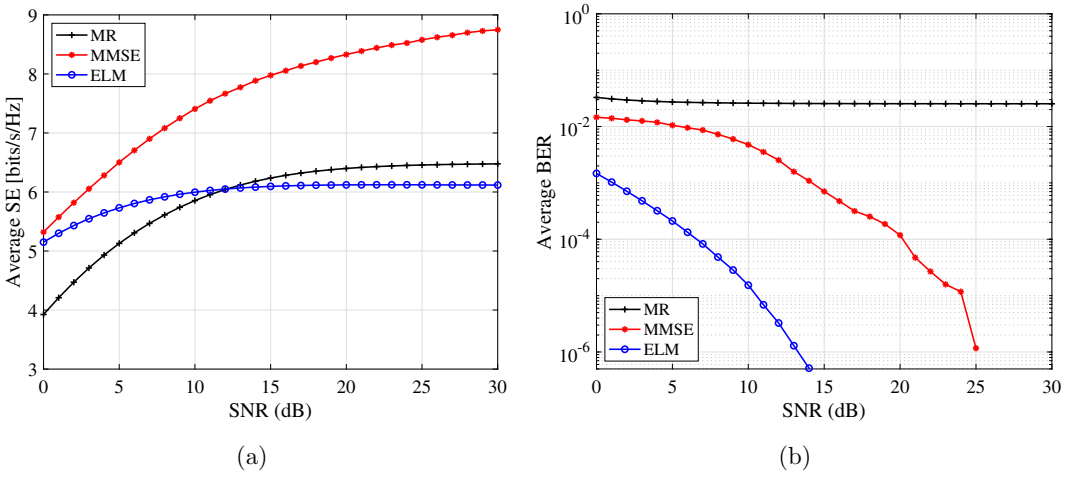

Fig. 4. Performance of evaluated detector schemes using QPSK modulation and 10 dB of EIRP. (a) Spectral efficiency. (b) Bit error rate.

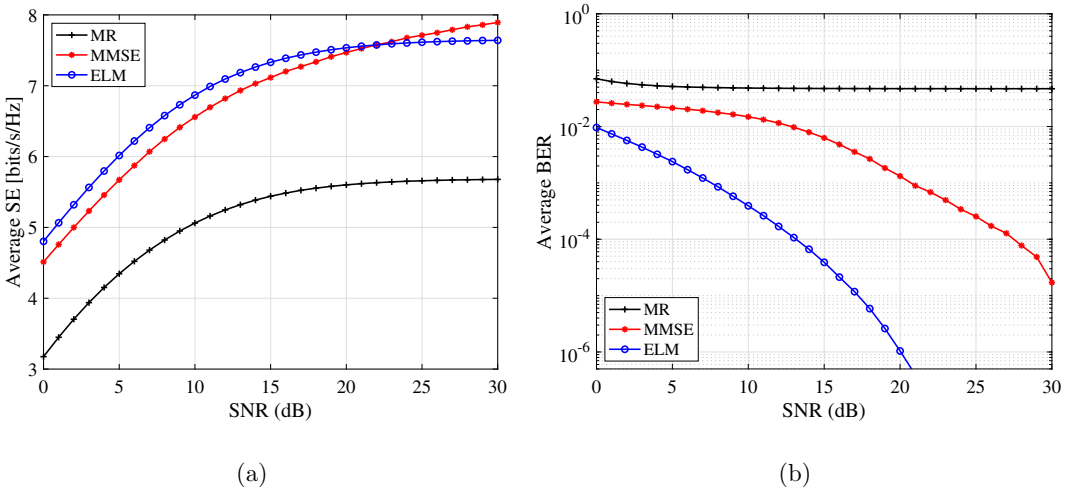

Fig. 5. Performance of evaluated detector schemes using 16-QAM modulation and 10 dB of EIRP. (a) Spectral efficiency. (b) Bit error rate.

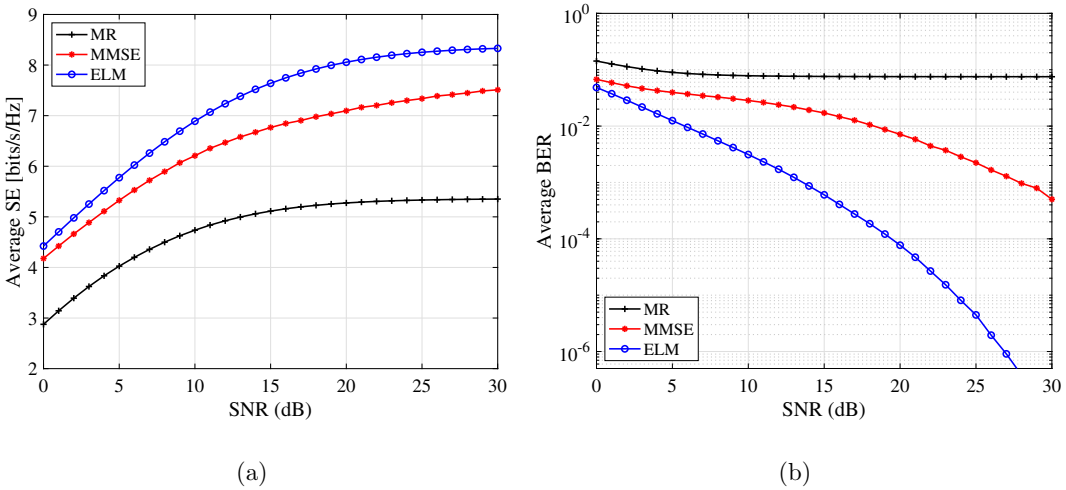

Fig. 6. Performance of evaluated detector schemes using 64-QAM modulation and 10 dB of EIRP. (a) Spectral efficiency. (b) Bit error rate.

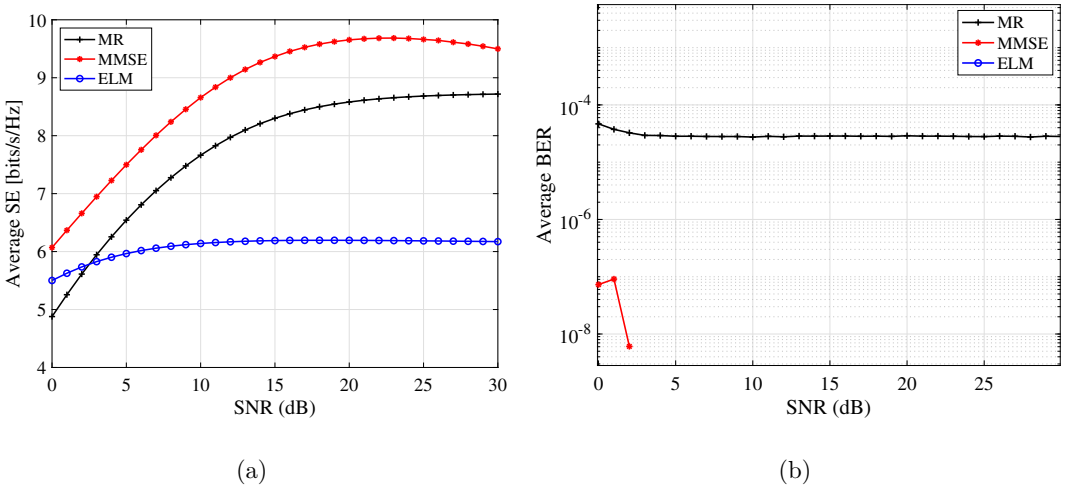

Fig. 7. Performance of evaluated detector schemes using QPSK modulation and 20 dB of EIRP. (a) Spectral efficiency. (b) Bit error rate.

dBm with the QPSK, 16QAM, and 64-QAM modulation schemes, respectively.

Figs. 7–9 show the MMSE detector presents higher SE, although the BER is higher than that obtained with the ELM method. Specifically, For the QPSK modulation scheme in Fig. 7, the ELM detector presents no BER. For 16- and 64-QAM modulations, the achieved BER of the ELM design is smaller than those of the compared methods. On the other hand, linear MIMO detectors, namely, MR and MMSE, require a minimum EIRP to achieve higher SE and therefore smaller BER.

Finally, Table 2 summarizes the number of floating-point operations required to implement the MR, MMSE, and ELM MIMO combining methods [6].

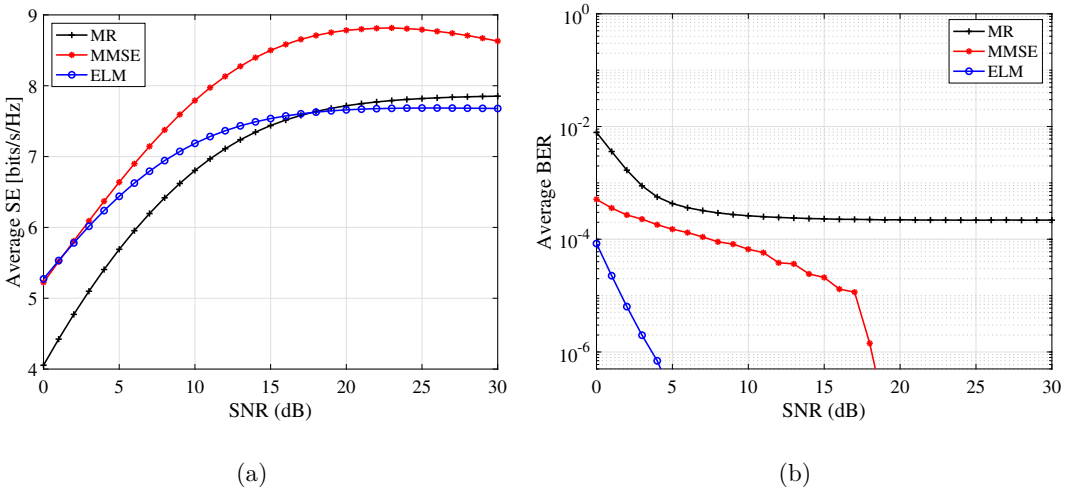

Fig. 8. Performance of evaluated detector schemes using 16-QAM modulation and 20 dB of EIRP. (a) Spectral efficiency. (b) Bit error rate.

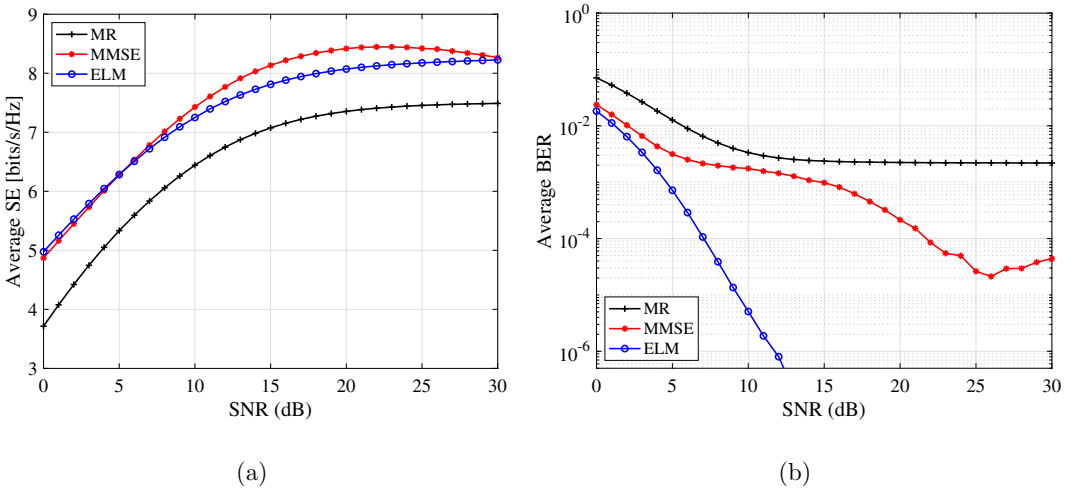

Fig. 9. Performance of evaluated detector schemes using 64-QAM modulation and 20 dB of EIRP. (a) Spectral efficiency. (b) Bit error rate.

Table 2
Floating-point operations of the different MIMO detectors.

Method	Combining vector operations
MR	$KN_s(4N_r - 1)$
MMSE	$N_s\left(N_r^3 + N_r^2(5K/2 + 2) + N_r(K + 1/2)\right)$
ELM	$K\left(L^3 + L^2(3N_s + 1/2) + L(2N_s - 1/2)\right)$

Based on the data presented in Table 2, for $K = 4, N_s = 792$, and $N_r = L = 64$, the ELM detector requires 40390528 floating-point operations, whereas the MR and MMSE detectors require 807840 and 246774528 operations, respectively. Therefore, the ELM scheme only requires 16% of the floating-point operations required by the MMSE detector. This reveals that the ELM scheme requires significantly fewer operations to function; therefore, supposes less computational complexity than the MMSE detector.

5. Discussion

As we can see in Section 4, the numerical results for SE are different from what we obtained for the BER. As an example, we can see that by changing the EIRP from 10 to 20 dB, the SE for the ELM method remains the same for QPSK modulation. However, the BER results differ since with an EIRP of 10 dB, the ELM method shows low BER, but with an EIRP of 20 dB, the BER is zero.

We see the same behavior in the results for 16-QAM and 64-QAM modulation schemes. As we know, the MMSE MIMO detector achieves higher SE with a higher EIRP. However, the BER results complement the SE, since the BER shows us the number of errors in the bit transmission domain.

The results show us that MIMO detectors like MMSE have the potential to achieve high spectral efficiency, but with high BER when the EIRP of the communications link is low. This is due to the interference effects since the MMSE detector can partially filter this perturbation. On the other hand, the proposed ELM detector presents the same SE for different EIRP links, but the BER results are smaller. These results show us that the ELM method can filter the interference effects better than the compared detectors in this study. However, with low EIRP links, the noise effects are noticeable and are still present.

6. Conclusion

The proposed ELM MIMO combining method can achieve a higher SE as well as a lower BER with a low EIRP power in the UL. Therefore, this method can significantly increase the coverage range of mm-wave communications, where the path loss is the main limiting factor. Additionally, the ELM method requires only 16 % of the floating-point

operations required for the MMSE detector. This reveals that the former not only achieves better wireless performance for systems with low power signals, but it is also characterized by having lower computational complexity.

Declaration of Competing Interest

The authors declare that they have no known competing financial interests or personal relationships that could have appeared to influence the work reported in this paper.

Acknowledgments

This work was supported by the Secretaría de Educación Pública (SEP)-Consejo Nacional de Ciencia y Tecnología (CONACyT) Research Project 255387, the School of Engineering and Sciences, the Telecommunications Research Focus Group at Tecnologico de Monterrey, and by ANID Project FONDECYT Regular 1211132. C. Vargas-Rosales is at the School of Engineering and Science, Tecnologico de Monterrey, Monterrey 64849, Mexico (e-mail: dfcarrera@ieee.org; cvargas@tec.mx). C. A. Azurdia-Meza is in the Department of Electrical Engineering, Universidad de Chile, Santiago 8370451, Chile (e-mail: cazurdia@ing.uchile.cl). M. Morocho-Yaguana is in the Department of Computer Science and Electronics, Universidad Tecnica Particular de Loja, Loja 110107, Ecuador (e-mail: mvmorocho@utpl.edu.ec).

References

[1] Fabre S. Hype Cycle for he Future of CSP Networks Infrastructure, 2020, Technical Report G00450437. Stamford, Connecticut, United States: Gartner Inc; 2020.
[2] A. Roessler, Pre-5G and 5G: Will the mmWave link work?, 5G Semiconductor Solutions-Infrastructure and Fixed Wireless Access (2018) 29.
[3] Bjornson E, Giselsson P. Two applications of deep learning in the physical layer of communication systems [lecture notes]. IEEE Signal Process. Mag. 2020;37:134–40.
[4] Carrera DF, Vargas-Rosales C, Yungaicela-Naula NM, Azpilicueta L. Comparative study of artificial neural network based channel equalization methods for mmwave communications. IEEE Access 2021;9:41678–87.
[5] Zabala-Blanco D, Mora M, Azurdia-Meza CA, Dehghan Firoozabadi A. Extreme learning machines to combat phase noise in RoF-OFDM schemes. Electronics 2019;8:921.
[6] Carrera DF, Zabala-Blanco D, Vargas-Rosales C, Azurdia-Meza CA. Extreme learning machine-based receiver for multi-user massive MIMO systems. IEEE Commun. Lett. 2020:1.
[7] Zhang J, Yu X, Letaief KB. Hybrid beamforming for 5G and beyond millimeter-wave systems: A holistic view. IEEE Open Journal of the Communications Society 2020;1:77–91.
[8] Gao D, Guo Q, Eldar YC. Massive mimo as an extreme learning machine. IEEE Trans. Veh. Technol. 2021;70:1046–50.
[9] Gao D, Guo Q, Jin M, Yu Y, Xi J. Adaptive extreme learning machine-based nonlinearity mitigation for LED communications. IEEE J. Sel. Top. Quantum Electron. 2020.
[10] Pal R, Sarawadekar K, Srinivas K. A decentralized beam selection for mmwave beamspace multi-user mimo system. AEU - International Journal of Electronics and Communications 2019;111:152884.
[11] Ubiali GA, Marinello JC, Abrão T. Energy-efficient flexible and fixed antenna selection methods for xl-mimo systems. AEU - International Journal of Electronics and Communications 2021;130:153568.
[12] Tao J, Xing J, Chen J, Zhang C, Fu S. Deep neural hybrid beamforming for multi-user mmwave massive mimo system. In: 2019 IEEE Global Conference on Signal and Information Processing (GlobalSIP); 2019. p. 1–5. https://doi.org/10.1109/GlobalSIP45357.2019.8969154.
[13] Li A, Masouros C. Hybrid precoding and combining design for millimeter-wave multi-user MIMO based on SVD. In: 2017 IEEE International Conference on Communications (ICC). IEEE; 2017. p. 1–6.
[14] Björnson E, Hoydis J, Sanguinetti L. Massive MIMO has unlimited capacity. IEEE Trans. Wireless Commun. 2017;17:574–90.
[15] Li H, Wang TQ, Huang X, Zhang JA, Guo YJ. Low-complexity multiuser receiver for massive hybrid array mmWave communications. IEEE Trans. Commun. 2019;67:3512–24.
[16] Carrera DF, Vargas-Rosales C, Villalpando-Hernandez R, Galaviz-Aguilar JA. Performance improvement for multi-user millimeter-wave massive mimo systems. IEEE Access 2020;8:87735–48.
[17] Zaidi A, Athley F, Medbo J, Gustavsson U, Durisi G, Chen X. 5G Physical Layer: Principles, Models and Technology Components. Academic Press; 2018.
[18] El Ayach O, Rajagopal S, Abu-Surra S, Pi Z, Heath RW. Spatially sparse precoding in millimeter wave MIMO systems. IEEE transactions on wireless communications 2014;13:1499–513.
[19] Khansefid A, Minn H. On channel estimation for massive MIMO with pilot contamination. IEEE Commun. Lett. 2015;19:1660–3.
[20] Carrera DF, Vargas-Rosales C, Azpilicueta L, Galaviz-Aguilar JA. Comparative study of channel estimators for massive MIMO 5G NR systems. IET Commun. 2020;14:1175–84.
[21] Rodríguez-Fernández J, González-Prelcic N, Venugopal K, Heath RW. Frequency-domain compressive channel estimation for frequency-selective hybrid millimeter wave mimo systems. IEEE Trans. Wireless Commun. 2018;17:2946–60.
[22] Sanguinetti L, Björnson E, Hoydis J. Towards massive MIMO 2.0: Understanding spatial correlation, interference suppression, and pilot contamination. IEEE Trans. Commun. 2019:1.
[23] Akdeniz MR, Liu Y, Samimi MK, Sun S, Rangan S, Rappaport TS, Erkip E. Millimeter wave channel modeling and cellular capacity evaluation. IEEE J. Sel. Areas Commun. 2014;32:1164–79.
[24] Ahmed I, Khammari H, Shahid A, Musa A, Kim KS, De Poorter E, Moerman I. A survey on hybrid beamforming techniques in 5G: Architecture and system model perspectives. IEEE Communications Surveys Tutorials 2018;20:3060–97.
[25] Zhang S, Tan W, Li Y. A survey of online sequential extreme learning machine. In: 2018 5th International Conference on Control, Decision and Information Technologies (CoDIT). IEEE; 2018. p. 45–50.
[26] Yang L, Zhao Q, Jing Y. Channel equalization and detection with ELM-based regressors for OFDM systems. IEEE Commun. Lett. 2020;24:86–9.
[27] Jaeckel S, Raschkowski L, Börner K, Thiele L, Burkhardt F, Eberlein E. Quasi deterministic radio channel generator user manual and documentation, Fraunhofer Heinrich Hertz Institute. Tech. Rep. 2016;v1:1–4.
[28] M. Tercero, P. von Wrycza, A. Amah, J. Widmer, M. Fresia, V. Frascolla, J. Lorca, T. Svensson, M.-H. Hamon, S.D. Roblot, et al., 5G systems: The mmMAGIC project perspective on use cases and challenges between 6–100 GHz, in: 2016 IEEE Wireless Communications and Networking Conference Workshops (WCNCW), IEEE, 2016, pp. 200–205.
[29] E. Degirmenci, EMF test report: Ericsson AIR 5121, Tech. Rep. GFTB-17:001589 Uen Rev B, Ericsson AB, Stockholm, Sweden, 2018.